THE JOURNAL OF PHYSICAL CHEMISTRY LETTERS
A JOURNAL OF THE AMERICAN CHEMICAL SOCIETY

pubs.acs.org/JPCL

Letter

# Theoretical Prediction of the 2-Dimensional Electronic Spectrum of Different Simulation Models of the Hydrated Electron

William R. Borrelli and Benjamin J. Schwartz*

Cite This: *J. Phys. Chem. Lett.* 2026, 17, 6030−6038

Read Online

ACCESS | Metrics & More | Article Recommendations | Supporting Information

**ABSTRACT:** Linear absorption spectroscopy has been the workhorse experimental method for probing hydrated electrons for the last several decades. There has been essentially no work, however, characterizing the nonlinear spectroscopy, such as the 2-dimensional electronic spectrum (2DES), of this species, despite the wealth of additional information that the 2DES provides. Nonlinear spectroscopy can directly measure homogeneous and inhomogeneous linewidths, quantify spectral diffusion, and probe the characteristic solvent dynamics that drive temporal line-shape evolution. This is particularly attractive for studying different simulation models of the hydrated electron. Most such models produce a roughly spherical charge density that predict a linear absorption spectrum in reasonable agreement with experiment, even though the solvent structure and dynamical fluctuations underlying these models are quite different. Thus, the temporal evolution of the 2DES signal provides an experimentally verifiable means to discriminate between different models and levels of theory for this species. In this work, we present the first theoretical predictions of the hydrated electron's 2DES. We show that two different one-electron models that produce very similar linear absorption spectra display distinct temporal dynamics of their 2DES signals. The results function not only as a prediction that can be compared directly to future experiments but also illustrate the utility of nonlinear spectroscopy in understanding the solvation dynamics of fully solvent-supported hydrated electron systems.

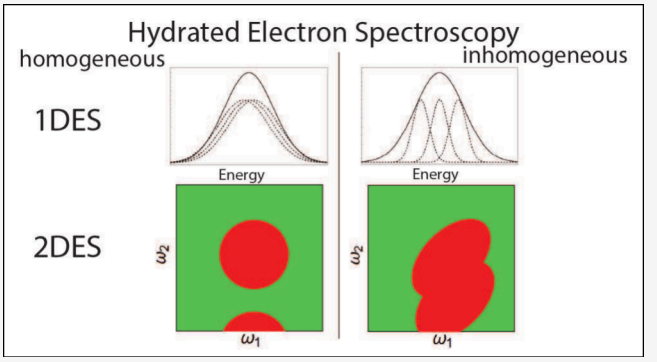




Hydrated electrons ($e^-_{hyd}$'s) are excess electrons that are stably solvated in liquid water. Hydrated electrons are important in a variety of fields, such as radiation chemistry,[1,2] and serve as incredibly strong reducing agents.[3,4] They also represent the simplest possible aqueous anion, one whose properties can be readily probed via various spectroscopies.[5−12] Since their discovery via absorption spectroscopy in the early 1960s,[6] the linear optical spectrum of the $e^-_{hyd}$ has been well characterized at numerous thermodynamic state points.[13] It is known that the hydrated electron's linear absorption spectrum has a Gauss-Lorentzian shape.[5,13,14] The maximum absorption of the $e^-_{hyd}$'s spectrum shifts modestly with temperature,[9,11,12,15] pressure,[13] and ionic strength,[16] all without any significant changes in shape. Despite all of this work on the spectroscopy of the hydrated electron, it is still not entirely clear what underlying structure and dynamics of the surrounding waters gives rise to the absorption spectrum under different conditions.

Given that the broad, featureless absorption spectrum provides little direct information about the structure of the $e^-_{hyd}$, most molecular information about this object comes from different types of molecular dynamics simulations. Until recently, most theoretical treatments of the hydrated electron relied on so-called mixed quantum-classical (MQC) simulations, where the water molecules of the system are treated classically, the excess electron is treated quantum mechanically, and the electron-water interaction is handled by a parametrized pseudopotential, several of which have been put forth in the literature.[17−21] In recent years, density functional theory (DFT) has become tenable for *ab initio* hydrated electron simulations of modest size and duration, and such simulations are now becoming relatively commonplace in the literature.[12,15,22−25] Nearly all of these simulations predict that the $e^-_{hyd}$ has a roughly spherical charge density that resides in a cavity in the water.[14,23] However, these different models predict different cavity sizes and local solvation structures,[17−19,23,26] which in turn lead to different predicted experimental observables. Unfortunately, because there is no definitive experimental probe of the hydrated electron's equilibrium solvation structure, simulations can only confront experiment through more indirect observables.

**Received:** April 20, 2026
**Revised:** May 12, 2026
**Accepted:** May 13, 2026
**Published:** May 18, 2026

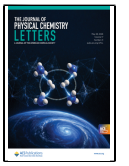





https://doi.org/10.1021/acs.jpclett.6c01291
*J. Phys. Chem. Lett.* 2026, 17, 6030−6038

Perhaps the easiest indirect observable to measure of the hydrated electron is its linear absorption spectrum, which is generally straightforward to compute from simulation. However, there are significant limitations as to the information that can be gleaned from the $e^-_{hyd}$'s absorption spectrum, as most simulation models that yield a roughly spherical excess electron density of the correct size (~2.5 Å radius of gyration, based on moment analysis of the experimental spectrum[27]) give a spectrum in reasonable agreement with experiment.[23] As examples, panel (a) of Figure 1 shows the $e^-_{hyd}$'s linear absorption spectrum from experiment (black curve) and two different MQC simulation models: one with a pseudopotential developed by Turi and Borgis (TB, blue curve)[17] and a reparameterized version of this potential designed to optimize polarization interactions against CCSD calculations (TBOpt, green curve).[19] Even though these models predict very different experimental observables, such as the molar solvation volume,[28,29] vertical detachment energy,[19,20] degree of ion pairing with salts,[25] temperature dependence,[11] time-resolved photoelectron spectroscopy,[10] and solvation entropy,[26] their simulated spectra have similar shapes and absorption maxima. We also note that a now-discredited noncavity $e^-_{hyd}$ model that we proposed over 15 years ago (not shown) also predicts a similar spectrum.[18] This means that it is not possible to use the experimental spectrum to distinguish the underlying structure of these models.

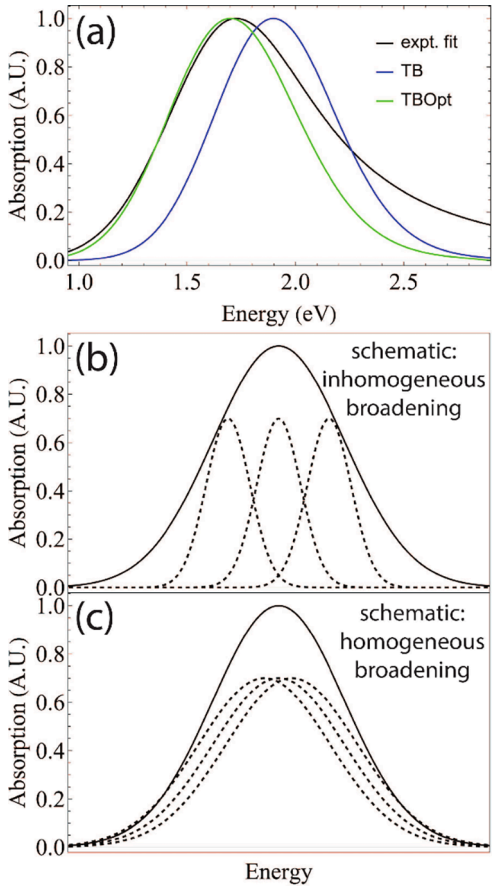


**Figure 1.** Panel (a) shows the $e^-_{hyd}$'s linear absorption spectrum from experiment (black curve)[32] and two MQC simulation models: the TB model[17] (blue curve) and the TBOpt model[19] (green curve). The linear spectra of both models are similar, despite having different underlying structures and solvent dynamics that lead to differences in many other predicted observables. (b,c) Schematic illustratiions of the Gauss-Lorentzian shape of the hydrated electron's absorption spectrum (solid curves) along with limiting possible contributions of the underlying individual $s \rightarrow p$ spectral contributions (dashed curves). Panel (b) shows a schematic spectrum where solvent motions do not cause the relative energies of the excited states to interchange quickly, leading to an inhomogeneously broadened spectrum where each sub-band could be resolved. Panel (c) shows the case of a mostly homogeneously broadened spectrum, where the relative energies of the three underlying transitions interchange on a time scale fast relative to the inverse of the absorption line width. The linear spectrum cannot distinguish between the two possible limiting cases in panels (b) and (c), but 2DES can directly reveal the time-scale of the underlying solvent fluctuations coupled to the different transitions.

This leads to the question of understanding the role of the solvent dynamics underlying the ground to excited-state energy gaps of the hydrated electron, which is what determines the width of the spectrum. Since the $e^-_{hyd}$'s spectroscopy is roughly that of a particle in a spherical box, it is dominated by three quasi-degenerate $s \rightarrow p$-like transitions. We note that the blue tail of the spectrum is believed to result from bound to continuum transitions[14,30] that are challenging to account for theoretically, which is why virtually all simulations of the hydrated electron underestimate the magnitude of the blue spectral tail. The nature of the main part of the absorption spectrum depends on the rate at which solvent fluctuations cause the three excited states to interchange roles. Figures 1b and c show a schematic of the optical absorption spectrum of the hydrated electron (solid curves) with two possible limiting sets of dynamics governing the three hypothetical underlying $s \rightarrow p$ excitation bands (dashed curves). If the solvent motions that split the degeneracy of the $p$-like states are slow, then the absorption spectrum would be inhomogeneously broadened, consisting of a superposition of three distinguishable sub-bands, as seen in panel (b). On the other hand, if solvent fluctuations scramble the energies of the three excited states faster than the inverse of the absorption line width, the so-called fast modulation limit,[31] then the spectrum is homogeneously broadened and one cannot resolve separate underlying bands, as depicted in panel (c).

Here, we propose that the inability of linear spectroscopy to distinguish between different molecular models of the $e^-_{hyd}$ can be overcome by using nonlinear spectroscopic methods, in this case, by examining the 2-dimensional electronic spectrum (2DES) of different simulation models. Two-dimensional electronic spectroscopy is a third-order spectroscopy technique that involves two pump pulses and one probe pulse. The first pulse creates an electronic coherence in the system, the second pulse creates an excited-state population, and the phase-resolved third pulse measures the corresponding absorption change. The time delays between the three laser pulses are denoted $t_1$, $t_2$, and $t_3$, and 2DES is measured as a function of $t_2$, the so-called 'waiting time', which is the time that the coherence evolves before being converted to an excited-state population. By varying $t_2$, one can thus resolve the characteristic solvent fluctuation time scales that modulate the 2DES signal and thus tease out the underlying broadening mechanisms at play.[33−36] This is because the method allows one to time-resolve dephasing of the coherences due to both fast fluctuations of the solvent environment (i.e., contributions that lead to homogeneous broadening) and those resulting


https://doi.org/10.1021/acs.jpclett.6c01291
J. Phys. Chem. Lett. 2026, 17, 6030−6038

from static disorder of the environment (leading to inhomogeneous broadening).

The interpretation of 2DES involves extracting all of the available information about what happens following excitation of a sample at one frequency (usually plotted on the horizontal axis) and subsequently probing the response at all possible frequencies (usually plotted on the vertical axis). Contributions to the 2DES signal include the ground-state bleach (GSB), where photoexcitation reduces the absorption of the ground-state population, stimulated emission (SE), where light induces emission from an excited state to the ground state, and excited-state absorption (ESA), which involves transitions between excited states (note that as described below, we neglect ESA in this work). The features along the diagonal of the 2-D spectrum ($\omega_{\text{pump}} = \omega_{\text{probe}}$) effectively recover the linear absorption spectrum (i.e., the response at the same frequency that was pumped), while off-diagonal peaks ($\omega_{\text{pump}} \neq \omega_{\text{probe}}$) indicate coupling between distinct underlying spectral features.

In a typical 2DES experiment, the SE signal will undergo a Stokes shift as a function of waiting time due to solvent reorganization that stabilizes the energy of the newly created excited state relative to the ground state. The contour width of the main GSB peak along the diagonal axis provides a measure of the inhomogeneous broadening ($\Delta$), while the antidiagonal width reports on homogeneous broadening ($\Gamma$). The decay of the center-line slope (CLS), which tracks the slope of a line connecting the frequencies of maximum signal as a function of waiting time, correlates well with the underlying energy gap relaxation dynamics. We show in what follows that the different $e^-_{\text{hyd}}$ simulation models with similar linear absorption spectra shown in Figure 1c give rise to significantly different 2DES, so that a 2DES experiment could readily distinguish between these (and potentially many other) models, providing new information about the hydrated electron and its underlying dynamics.

The question of whether or not the spectrum of the $e^-_{\text{hyd}}$ is more homogeneously or inhomogeneously broadened has been investigated in previous work. Early simulation work predicted an inhomogeneously broadened spectrum, and argued that the inhomogeneity could be resolved via a polarized transient hole-burning (pTHB) experiment.[37,38] When the first pTHB experiments were performed, they appeared to support this inhomogeneous prediction.[39] More recent experimental work, based on both pTHB[25,31,40−42] and resonance Raman spectroscopy,[43] in contrast, concluded that the hydrated electron's absorption spectrum is homogeneously broadened up to a time scale of ∼20 fs. Disconcertingly, nearly every simulation model of this species investigated to date (with the possible exceptions of TBOpt[19] and the now-discredited noncavity model[18]), including those based on DFT, predicts a much more inhomogeneously broadened spectrum than what is seen experimentally.[25] The experiments done to date, however, do not provide a full picture of the underlying time scales of inhomogeneous and homogeneous broadening in this system; here, we propose that these could be directly quantified from a 2DES experiment.

As a spectroscopic technique, 2DES could provide a richer picture of the solvent fluctuations underlying the hydrated electron's spectroscopy compared to previous experiments. For example, although pTHB does provide some information about the degree of homogeneous or inhomogeneous broadening, the underlying dynamics being probed in this experiment is the transition dipole reorientation correlation function rather than the energy gap correlation function,[25] and it is not clear that these two correlation functions should be the same. Wiersma and co-workers performed photon echo (PE) experiments on the $e^-_{\text{hyd}}$,[41] but the few-fs decay they saw resulted primarily from the large magnitude of the underlying Stokes shift, which leads to rapid dephasing, rather than from the dynamics of the underlying solvent fluctuations.[44] Fluorescence yield experiments also have provided insight into the hydrated electron's excited-state lifetime,[9,43] but again, do not reveal the energy-gap correlation function. In general, PE experiments measure a phase-matched signal that primarily probes dephasing, inhomogeneous broadening, and spectral diffusion, whereas 2DES captures both rephasing and nonrephasing contributions and resolves cross-coupling between electronic states. In fact, 2DES contains all of the information from 3-pulse photon echo, pump/probe, and transient grating spectroscopies. For these reasons, we believe that the 2DES is the most well-suited experiment for understanding the spectroscopy of the hydrated electron.

The purpose of this work is to answer the following question: how can 2DES differentiate between two simulation models of the $e^-_{\text{hyd}}$ that produce very similar linear spectra? As far as we are aware, the 2DES of the hydrated electron has not been measured experimentally, so this work provides a set of predictions for what might be seen based on different underlying models. Thus, in what follows, we present theoretical predictions of the 2DES of both the TB and TBOpt MQC simulation models of the $e^-_{\text{hyd}}$. We show that both models display readily distinguishable 2DES relaxation behavior: the TBOpt model, which has faster underlying solvent fluctuations, shows the most homogeneous behavior, while the TB model shows much slower fluctuations that would give rise to readily observable inhomogeneous behavior. Moreover, predicted differences in the 2DES dynamics should be apparent on the tens of femotoseconds time-scale. These results not only function as detailed predictions for this nonlinear spectroscopic signal but also show that the 2DES is potentially the most powerful spectroscopic method for differentiating between simulation models of this species.

To compute a 2DES signal, one needs to construct the third-order nonlinear response function, $R^{(3)}$. The cumulant approach is particularly suited to modeling systems with explicit solvent,[34,35] and this is the approach we take in this work. The cumulant approach expresses the response function as an infinite cumulant expansion of energy-gap fluctuations ($\delta U = (\omega_e - \omega_g) - \omega_{eg}^{\text{avg}}$) sampled from MD. The vertical energy gap between the ground state and the excited state is given by $\omega_e - \omega_g$, while $\omega_{eg}^{\text{avg}}$ is the average energy gap. If the energy gap fluctuations obey Gaussian statistics, cumulants beyond order 2 vanish.[34,45] The 2DES signal can then be written in terms of the rephasing and nonrephasing functions ($R_1$, $R_2$, $R_3$, $R_4$):[34,45]

$$S_{\text{2DES}}(\omega_3, t_{\text{delay}}, \omega_1) \propto \text{Re} \int_0^\infty dt_3 \int_0^\infty dt_1 [e^{i\omega_3 t_3 + i\omega_1 t_1} \times (R_1(t_3, t_{\text{delay}}, t_1) + R_4(t_3, t_{\text{delay}}, t_1)) + e^{-i\omega_3 t_3 + i\omega_1 t_1}(R_2(t_3, t_{\text{delay}}, t_1) + R_3(t_3, t_{\text{delay}}, t_1))] \quad (1)$$

which themselves can be written in terms of sums of the second-order cumulant line-shape ($g_2(t)$). The second-order



https://doi.org/10.1021/acs.jpclett.6c01291
J. Phys. Chem. Lett. 2026, 17, 6030−6038

cumulant line-shape function can be derived from an integral over the spectral density ($J(\omega)$):[34,45]

$$g_2(t) = \frac{1}{\pi}\int_0^\infty d\omega \frac{J(\omega)}{\omega^2}[\coth\left(\frac{\beta\omega}{2}\right)[1 - \cos(\omega t)] - (i[\sin(\omega t) - \omega t])] \quad (2)$$

which can be approximated as the Fourier transform of the energy-gap autocorrelation function:[34,45]

$$J(\omega) = i\theta(\omega)\int dt\, e^{i\omega t}\, \mathrm{Im}\, C_{\delta U}(t) \quad (3)$$

where $C_{\delta U}(t) = \langle \delta U(0)\delta U(t)\rangle$, and $\theta(\omega)$ is the Heaviside function. We note that in order to substitute a classical time-correlation function for $C_{\delta U}(t)$, we use the quantum correction factor $(\beta\omega)/2$.[35,46] 2DES signals were calculated separately for each excited state and then added together to obtain the total signal. In the SI we show that combining the contributions from each state at the response function level gives a nearly identical result.

To implement this method for the hydrated electron simulated at the mixed quantum-classical level of theory, we ran 4 ns of equilibrium dynamics with the TB[17] $e^-_{hyd}$ model and 3.75 ns of dynamics with the TBOpt[19] model. The excess electron was treated quantum mechanically with a grid basis (16 × 16 × 16 grid), and 499 classical water molecules were treated with the SPC/Flex[47] water model. This use of a flexible water model means that our computed spectral densities will contain contributions from the intramolecular modes of waters near the hydrated electron. At each time step, the ground and first 3 excited states were calculated and an adiabatic following algorithm was implemented to track the identity of each state over time (see the SI for details). This was done to account for the fact that the relative energies of the three nearly degenerate excited states scramble due to solvent fluctuations. To faithfully construct an energy-gap autocorrelation function for each transition, the identity of each excited state has to be tracked in order to account for decorrelation due to crossing of excited-state energies. Our adiabatic following scheme assigned the identity of the excited states by maximizing wave function overlap over the entire trajectory. Energy gaps were sampled every 0.5 fs for construction of energy-gap fluctuation autocorrelation functions.

The central quantity in computing the 2DES with the cumulant approach is the energy-gap time autocorrelation function, $C_{\delta U}(\tau) = \langle \delta U(0)\delta U(\tau)\rangle$, where $\delta U$ is the deviation of the energy gap from its average value and the angle brackets denote an ensemble average; this correlation function is readily obtained from molecular dynamics simulations. Figure 2a shows the normalized $e^-_{hyd}$ energy gap fluctuation autocorrelation functions for both the TB (blue curve) and TBOpt (green curve) $e^-_{hyd}$ models, with an applied exponential damping function ($\tau$ = 250 fs). We note that damping of the energy-gap autocorrelation function is standard in the field to ensure numerical stability of its Fourier transform.[34] The standard deviation of the energy gap fluctuations are 0.257 eV for TB and 0.260 eV for TBOpt. We only compute ground to excited-state energy gaps (no ESA) and we neglect any excited-state cross-coherences. In the SI, we show that including the cross-coherences makes minimal difference to the resulting spectra due to the fact that the transition dipole prefactor is negligible in magnitude compared to the diagonal terms. We also show that the autocorrelation functions for each of the three *p*-like excited states become identical given long enough sampling and the correct adiabatic following.

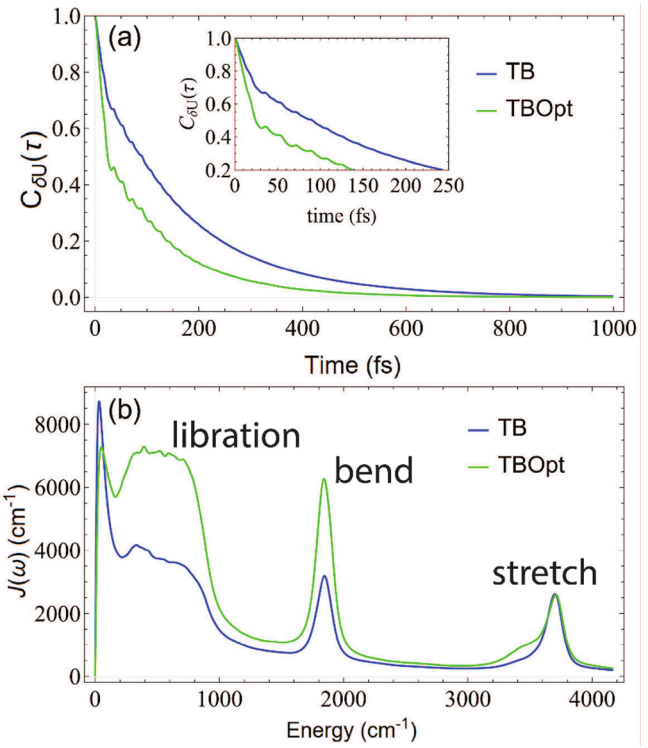


**Figure 2.** (a) Normalized energy-gap fluctuation autocorrelation functions, damped with a decaying exponential, for the TB (blue curve) and TBOpt (green curve) $e^-_{hyd}$ models. The inset shows the same plot over an expanded time window. Both models show significant inertial relaxation in the first ∼40 fs followed by a slower biexponential decay, as often seen in aqueous environments. TBOpt has a more significant inertial relaxation compared to TB, and the overall correlation function decays on a faster time scale. We note that the standard deviation of the energy gap fluctuations are 0.257 eV for TB and 0.260 eV for TBOpt. Panel (b) shows the spectral densities for the TB (blue curve) and TBOpt (green curve) $e^-_{hyd}$ models resulting from a Fourier transform of the correlation functions in (a); low-frequency water translational and librational modes, water bends, and O−H stretches modulate the hydrated electron's energy gaps. The TBOpt model shows more significant librational and bending contributions compared to TB, a result of the more enhanced polarization potential and fluctional solvation structure of this model.

It has been previously shown that the TBOpt model has a more fluctional solvation structure compared to the TB model, with faster solvation dynamics of the waters in the first solvation shell.[17,19,25,26] Indeed, within the first ∼40 fs (panel a inset), both models show a significant inertial relaxation. The amplitude of this inertial relaxation is about twice as large for TBOpt as for TB. After this rapid relaxation, both models exhibit a slower decay that shows the characteristic biexponential behavior common for solutes in aqueous environments.[48] These different relaxation time scales for the different simulation models should be readily evident in the 2DES in both how quickly the stimulated emission (SE) signal red-shifts out of the spectral window and how quickly the center-line-slope (CLS) of the main GSB feature decays.[49]

Figure 2b shows the spectral densities, $J(\omega)$, that result from a Fourier transform of the energy-gap autocorrelation functions for both $e^-_{hyd}$ models; the Fourier transforms are


https://doi.org/10.1021/acs.jpclett.6c01291
J. Phys. Chem. Lett. 2026, 17, 6030−6038

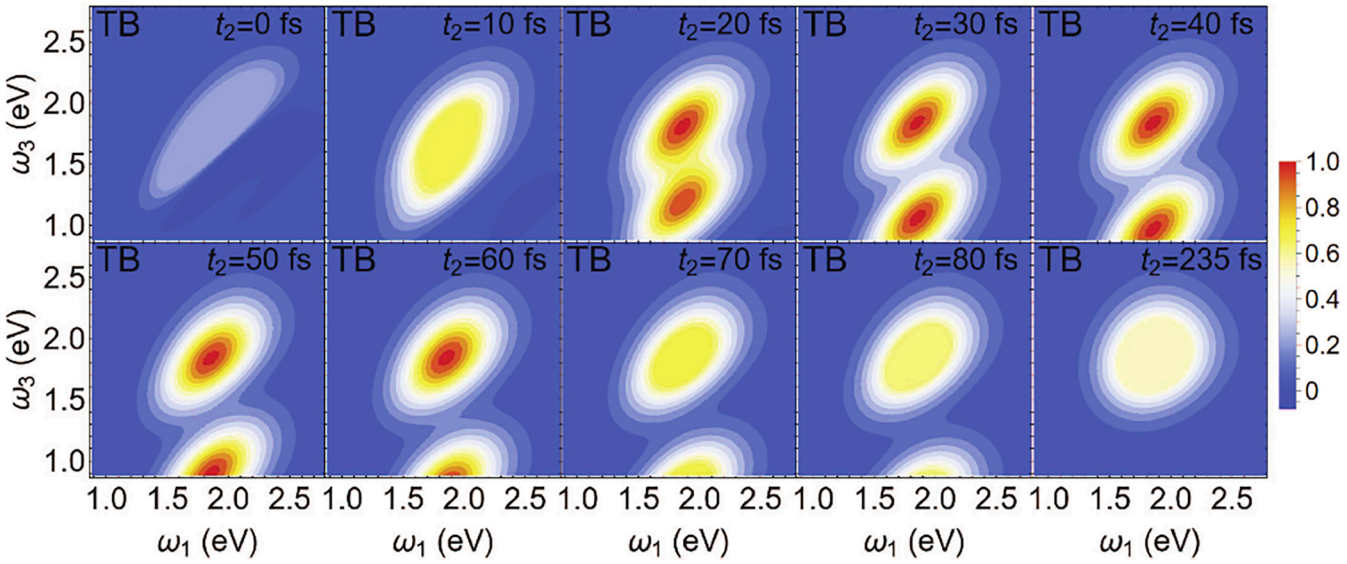


**Figure 3.** Calculated 2DES of the TB model as a function of waiting time ($t_2$) for relatively short population times. Within 50 fs the stimulated emission begins to red-shift off of the spectral window and the main GSB peak starts to become more circular. After 80 fs, the stimulated emission is still not completely out of the spectral window and the main GSB peak is not completely circular, as seen later at $t_2$ = 235 fs.

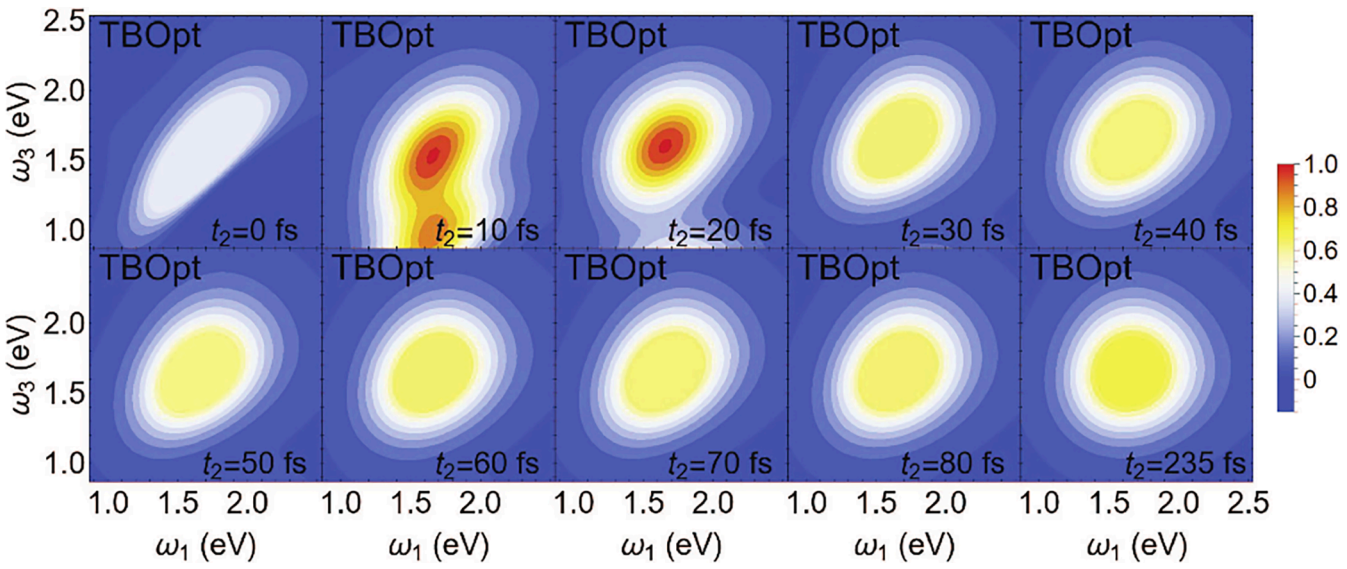


**Figure 4.** Calculated 2DES of the TBOpt model as a function of waiting time ($t_2$) for relatively short population times. Within 50 fs the stimulated emission has completely red-shifted out of the spectral window and the main GSB peak has become significantly more round compared to the TB model.

purely real because the underlying correlations functions are real and symmetric in time. The spectral densities encode the frequencies of the solvent modes that modulate the energy gaps of the hydrated electron. The lower-energy broad features near 800 $cm^{-1}$ correspond to water librations, the peak near 1900 $cm^{-1}$ corresponds to the intramolecular water bend, and the feature near 3700 $cm^{-1}$ is due to O−H stretching motions. Interestingly, the TBOpt $e^-_{hyd}$ shows a stronger weighting of the low-frequency librational and intramolecular bends compared to TB. Since the core static-exchange part of the pseudopotential is the same for both the TB and TBOpt models, these differences must arise from the different polarization potentials, which produces a more fluctional solvation structure for TBOpt that allows the first-shell waters to sample a much greater range of orientations compared to TB.[19,26] It is likely that this enhanced librational freedom is what allows for better coupling between the bending mode and the energy gap for the TBOpt model.

With these spectral densities in hand, we can now compute the 2DES signal for each model. As discussed in the Methods section and SI, an integral of the spectral density yields the second-order cumulant line-shape function, $g_2(t)$. The rephasing and nonrephasing functions that correspond to all of the allowed Liouville pathways for the 2DES experiment are integrals over sums of the line-shape function, and finally the double Fourier transform of the response function yields the 2DES signal.[34,35,45,50] Figure 3 shows the 2DES signal for the TB $e^-_{hyd}$ at waiting times $t_2$ < 250 fs. The $\omega_1$ axis corresponds to the pump frequency while the $\omega_2$ axis corresponds to the probe frequency. At $t_2$ = 0, we see the ground-state bleach (GSB)


https://doi.org/10.1021/acs.jpclett.6c01291
J. Phys. Chem. Lett. 2026, 17, 6030−6038

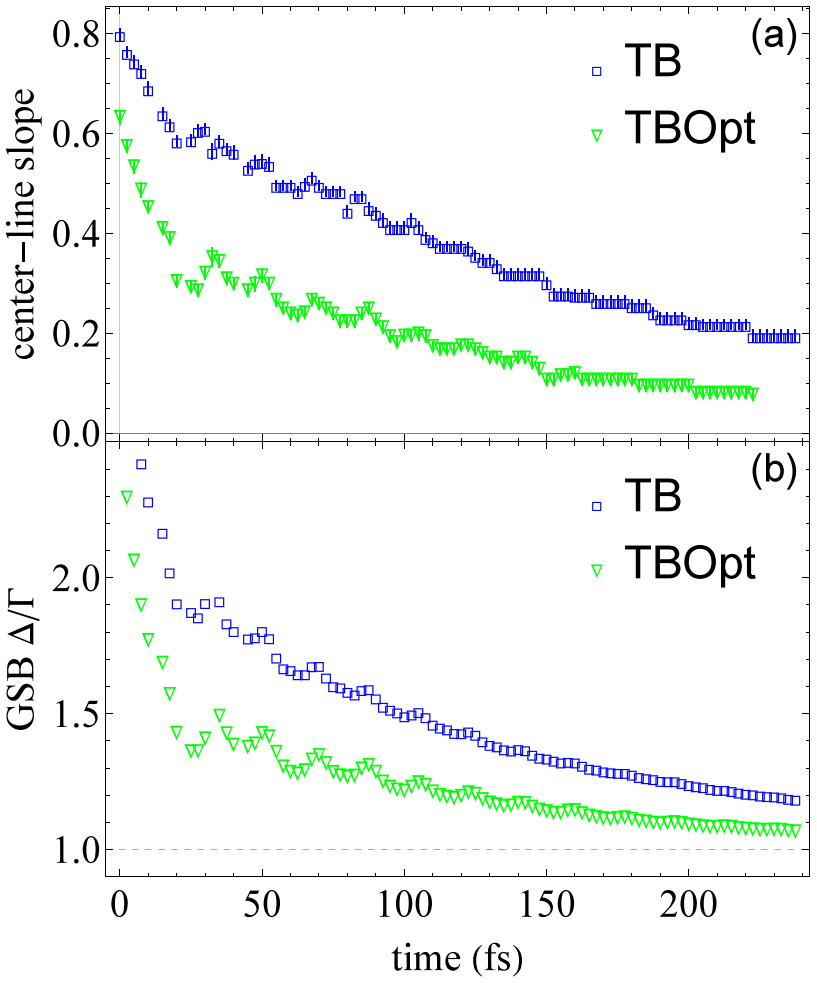


**Figure 5.** (a) Center-line slope (CLS) dynamics of the TB $e^-_{hyd}$ (blue open squares) and TBOpt (green open triangles) $e^-_{hyd}$ models, calculated from the 2DES signals in Figures 3 and 4. At $t_2 = 0$ the CLS starts near 1 as the 2DES signal is elongated along the diagonal. As $t_2$ increases, the main GSB feature of the spectrum rounds and the CLS approaches 0. The TBOpt CLS clearly relaxes on a faster time scale than TB. Uncertainties are the estimated standard error of the linear slope fit to the signal at each waiting time. Data points resulting from linear fits that had $R^2 < 0.7$ were omitted from the CLS curves. (b) Ratio of the inhomogeneous (diagonal) to homogeneous (off-diagonal) line widths of the 2DES signal GSB feature as a function of waiting time for the TB (blue markers) and TBOpt (green markers) $e^-_{hyd}$ models, which better reflect the original underlying energy gap correlation functions in Figure 2.

signal elongated along the diagonal, indicating inhomogeneity at the earliest times. After ∼20 fs, the stimulated emission (SE) signal has red-shifted enough to become a distinct feature, which then continues to red-shift out of the spectral window as the waiting time increases. Even by $t_2 = 80$ fs, the SE signal has not fully left the window and the main GSB feature has not become fully circular, indicating persistent inhomogeneity in the spectroscopy.

On the other hand, the TBOpt hydrated electron 2DES signal, shown in Figure 4, reflects the much faster underlying solvent dynamics of this model. The SE peak becomes distinct as early as 10 fs waiting time, and by $t_2 = 30$ fs, the SE signal has shifted completely out of the spectral window. The remaining main GSB peak has become quite circular and remains relatively unchanged from $t_2 = 30$ fs up to $t_2 = 80$ fs, something that is more consistent with a homogeneously broadened spectrum on this time scale. Given how similar their linear absorption spectra are, it is clear that 2DES reveals stark differences in the solvent motions underlying the TB and TBOpt $e^-_{hyd}$ simulation models.

These different underlying dynamics of the TB and TBOpt $e^-_{hyd}$ models can be further probed by investigating the center-line-slope (CLS) of the 2D spectra. The CLS is calculated by finding the probe frequency with the largest signal at a given pump frequency. The slope of the line connecting these points as a function of waiting time is the CLS. The dynamics of this slope should roughly reflect the relaxation of the underlying energy gap correlations.[49] At $t_2 = 0$, where the main 2DES peak is elongated along the diagonal, the CLS is close to 1, and as this 2DES feature becomes more circular, the CLS decays to 0. Figure 5(a) shows the CLS decay plots for both models calculated directly from the 2DES signals in Figures 3 and 4. The missing data points correspond to waiting times where the $R^2$ of the linear fit was below 0.7. Clearly, TBOpt shows a much faster decay of the CLS compared to TB, decaying to nearly zero after ∼150 fs. On the other hand, the TB model CLS only decays to ∼0.3 by 250 fs. As expected,[49] these curves do somewhat resemble the inset of Figure 2, verifying that one can use the CLS of 2DES signals to roughly extract the underlying solvent relaxation dynamics.



https://doi.org/10.1021/acs.jpclett.6c01291
J. Phys. Chem. Lett. 2026, 17, 6030−6038

Figure 5(b) shows an alternate means of extracting the underlying solvent dynamics from 2DES signal, in this case, by examining the ratio of the diagonal (inhomogeneous) line-width ($\Delta$) to the off-diagonal (homogeneous) line-width ($\Gamma$) of the main GSB peak.[51] We calculated this by finding the major and minor axis widths of the 0.20 2DES contour fit to an ellipse. At short waiting times, when the 2DES signal is elongated along the diagonal, this ratio is greater than 1, and as the spectrum becomes circular at longer waiting times, this ratio tends to a value of unity. Similar to the CLS, the TBOpt $\bar{e}_{hyd}$ shows a very quick decay of the broadening ratio, approaching unity after ~150 fs. The TB $\bar{e}_{hyd}$, on the other hand, shows a slower decay, having not yet reached a value of 1 by the end of the 250 fs time window. Although we do not present 2DES results for DFT-simulated hydrated electrons here (we refer the reader to the SI for a discussion of the computational challenges involved), previous work has established, at least for the commonly used PBEh-D3 density functional, that solvent fluctuations around the electron are significantly slower than those of both of these MQC-based models.[25,26] This would suggest that the resulting 2DES dynamics for the PBEh-D3 hydrated electron would be correspondingly slower than TB and TBOpt, so that a 2DES experiment could readily distinguish between the TB, TBOpt and PBEh-D3-based hydrated electron models.

We note that the CLS and broadening ratio curves in Figure 5 were calculated using only the GSB contribution to the spectrum, as this gives the cleanest signal. Of course, this would not be possible experimentally since the SE and ESA signals would complicate a direct calculation of both of these measures, particularly on the red side of the spectrum where both of these contributions occur. However, we showed in previous experimental and theoretical work[9,11] that the blue side of the transient absorption bleach perfectly overlaps the ground-state equilibrium spectrum at early times. Moreover, experiments from other groups have shown that the initial ESA signal occurs in the terahertz and only blue-shifts toward the ground-state spectrum over tens to hundreds of femtoseconds.[7,8] This means that the blue side of the transient spectrum is devoid of both SE and ESA[37] on the time scales over which we compute the 2DES. In the SI, we show that the broadening ratio also can be obtained by fitting only the blue side of the 2DES signal, yielding qualitatively similar curves to those in Figure 5b, and we propose that this would provide the best way to compare a future 2DES experiment to the results presented here.

In summary, this work presents the first theoretical prediction of the 2DES for the hydrated electron, calculated with two commonly used cavity-forming simulation models for this species. Although both of these models produce similar linear absorption spectra, we find that each yields a highly distinct 2DES due to the very different underlying solvent dynamics. The TB model showed a SE signal that initially shifts moderately quickly, and then takes a longer time (>250 fs) to lose memory of the initial conditions. Conversely, the TBOpt model showed very rapid shifting of the SE signal (that would be difficult to resolve with the 10 fs time-resolution that is currently state-of-the-art experimentally) as well as much more rapid loss of initial memory. 2DES spectroscopy is a highly sensitive tool for spectroscopically probing the underlying solvation dynamics, allowing it to differentiate between different hydrated electron simulation models, even those that produce a cavity structure. This emphasizes that not all cavity-forming models of the hydrated electron are equal, and we hope that this work inspires an experimental measurement of the 2DES to better discriminate between models for this species. Future work aims to incorporate the effects of polarized light on the 2DES as well as how higher-order cumulants change the spectral line-shape.

## ■ ASSOCIATED CONTENT

### Data Availability Statement

All data necessary to reproduce the results presented here are available in the following online repository: 10.5061/dryad.jq2bvq8r1.

### Supporting Information

The Supporting Information is available free of charge at https://pubs.acs.org/doi/10.1021/acs.jpclett.6c01291.

The Supporting Information document contains details on our adiabatic following algorithm, 2DES calculations, and spectral dynamics analyses

## ■ AUTHOR INFORMATION


### Corresponding Author

**Benjamin J. Schwartz** − *Department of Chemistry and Biochemistry, University of California Los Angeles, Los Angeles, California 90095-1569, United States;* orcid.org/0000-0003-3257-9152; Email: bjs@g.ucla.edu

### Author

**William R. Borrelli** − *Department of Chemistry and Biochemistry, University of California Los Angeles, Los Angeles, California 90095-1569, United States*

Complete contact information is available at: https://pubs.acs.org/10.1021/acs.jpclett.6c01291


### Notes

The authors declare no competing financial interest.

## ■ ACKNOWLEDGMENTS

This work was supported by the National Science Foundation, under Grant CHE-2247583. Partial support for W. R. B. was provided by the U.S. Department of Energy, Basic Energy Sciences Condensed-Phase and Interfacial Molecular Science Program, under Grant DE-SC0017800. Computational resources were provided by the University of California, Los Angeles (UCLA) Institute for Digital Research and Education and Extreme Science and Engineering Discovery Environment (XSEDE), under Computational Project TG-CHE170065. The authors thank Profs. Tom Oliver and Tim Zuehlsdorff for helpful discussions.

## ■ REFERENCES

(1) Sopena Moros, A.; et al. Tracking Cavity Formation in Electron Solvation: Insights from X-ray Spectroscopy and Theory. *J. Am. Chem. Soc.* **2024**, *146*, 3262−3269.

(2) Marin, T. W.; Jonah, C. D.; Bartels, D. M. Reaction of OH* radicals with H2 in sub-critical water. *Chem. Phys. Lett.* **2003**, *371*, 144−149.

(3) Singh, P.; Lal, N.; Shaikh, A. C. Solvated Electrons: Dynamic Reductant in Visible Light Photoredox Catalysis. *Advanced Synthesis & Catalysis* **2024**, *366*, 1906−1921.

(4) Fennell, B. D.; Fowler, D.; Mezyk, S. P.; McKay, G. Reactivity of Dissolved Organic Matter with the Hydrated Electron: Implications for Treatment of Chemical Contaminants in Water with Advanced Reduction Processes. *Environ. Sci. Technol.* **2023**, *57*, 7634−7643.
(5) Hart, E. J. The Hydrated Electron. *Science* **1964**, *146*, 19−25.
(6) Hart, E. J.; Boag, J. W. Absorption Spectrum of the Hydrated Electron in Water and in Aqueous Solutions. *J. Am. Chem. Soc.* **1962**, *84*, 4090−4095.
(7) Novelli, F.; Chen, K.; Buchmann, A.; Ockelmann, T.; Hoberg, C.; Head-Gordon, T.; Havenith, M. The birth and evolution of solvated electrons in the water. *Proc. Natl. Acad. Sci. U. S. A.* **2023**, *120*, No. e2216480120.
(8) Woerner, M.; Fingerhut, B. P.; Elsaesser, T. Field-Induced Electron Generation in Water: Solvation Dynamics and Many-Body Interactions. *J. Phys. Chem. B* **2022**, *126*, 2621−2634.
(9) Farr, E. P.; Zho, C.-C.; Challa, J. R.; Schwartz, B. J. Temperature dependence of the hydrated electron's excited-state relaxation. II. Elucidating the relaxation mechanism through ultrafast transient absorption and stimulated emission spectroscopy. *J. Chem. Phys.* **2017**, *147*, 74504.
(10) Shreve, A. T.; Yen, T. A.; Neumark, D. M. Photoelectron spectroscopy of hydrated electrons. *Chem. Phys. Lett.* **2010**, *493*, 216−219.
(11) Zho, C.-C.; Farr, E. P.; Glover, W. J.; Schwartz, B. J. Temperature dependence of the hydrated electron's excited-state relaxation. I. Simulation predictions of resonance Raman and pump-probe transient absorption spectra of cavity and non-cavity models. *J. Chem. Phys.* **2017**, *147*, 74503.
(12) Lan, J.; Rybkin, V. V.; Pasquarello, A. Temperature Dependent Properties of the Aqueous Electron. *Angew. Chem., Int. Ed.* **2022**, *61*, No. e202209398.
(13) Bartels, D. M.; Takahashi, K.; Cline, J. A.; Marin, T. W.; Jonah, C. D. Pulse Radiolysis of Supercritical Water. 3. Spectrum and Thermodynamics of the Hydrated Electron. *J. Phys. Chem. A* **2005**, *109*, 1299−1307.
(14) Herbert, J. M. Structure of the aqueous electron. *Phys. Chem. Chem. Phys.* **2019**, *21*, 20538−20565.
(15) Park, S. J.; Schwartz, B. J. Understanding the Temperature Dependence and Finite Size Effects in Ab Initio MD Simulations of the Hydrated Electron. *J. Chem. Theory Comput.* **2022**, *18*, 4973−4982.
(16) Bonin, J.; Lampre, I.; Mostafavi, M. Absorption spectrum of the hydrated electron paired with nonreactive metal cations. *Radiat. Phys. Chem.* **2005**, *74*, 288−296.
(17) Turi, L.; Borgis, D. Analytical investigations of an electron−water molecule pseudopotential. II. Development of a new pair potential and molecular dynamics simulations. *J. Chem. Phys.* **2002**, *117*, 6186−6195.
(18) Larsen, R. E.; Glover, W. J.; Schwartz, B. J. Does the Hydrated Electron Occupy a Cavity? *Science* **2010**, *329*, 65−69.
(19) Glover, W. J.; Schwartz, B. J. Short-Range Electron Correlation Stabilizes Noncavity Solvation of the Hydrated Electron. *J. Chem. Theory Comput.* **2016**, *12*, 5117−5131.
(20) Neupane, P.; Bartels, D. M.; Thompson, W. H. Empirically Optimized One-Electron Pseudopotential for the Hydrated Electron: A Proof-of-Concept Study. *J. Phys. Chem. B* **2023**, *127*, 7361−7371.
(21) Neria, E.; Nitzan, A.; Barnett, R. N.; Landman, U. Quantum dynamical simulations of nonadiabatic processes: Solvation dynamics of the hydrated electron. *Phys. Rev. Lett.* **1991**, *67*, 1011−1014.
(22) Rybkin, V. V. Mechanism of Aqueous Carbon Dioxide Reduction by the Solvated Electron. *J. Phys. Chem. B* **2020**, *124*, 10435−10441.
(23) Borrelli, W. R.; Liu, X.; Schwartz, B. J. How the choice of exchange−correlation functional affects DFT-based simulations of the hydrated electron. *J. Chem. Phys.* **2025**, *162*, 110901.
(24) Ambrosio, F.; Miceli, G.; Pasquarello, A. Electronic Levels of Excess Electrons in Liquid Water. *J. Phys. Chem. Lett.* **2017**, *8*, 2055−2059.
(25) Park, S. J.; Schwartz, B. J. How Ions Break Local Symmetry: Simulations of Polarized Transient Hole Burning for Different Models of the Hydrated Electron in Contact Pairs with Na+. *J. Phys. Chem. Lett.* **2023**, *14*, 3014−3022.
(26) Borrelli, W. R.; Liu, X.; Schwartz, B. J. The Solvation Entropy of Different Simulation Models of the Hydrated Electron. *J. Phys. Chem. Lett.* **2026**, *17*, 1899.
(27) Bartels, D. M. Moment analysis of hydrated electron cluster spectra: Surface or internal states? *J. Chem. Phys.* **2001**, *115*, 4404−4405.
(28) Borrelli, W. R.; Mei, K. J.; Park, S. J.; Schwartz, B. J. Partial Molar Solvation Volume of the Hydrated Electron Simulated Via DFT. *J. Phys. Chem. B* **2024**, *128*, 2425−2431.
(29) Neupane, P.; Bartels, D. M.; Thompson, W. H. Relation between the Hydrated Electron Solvation Structure and Its Partial Molar Volume. *J. Phys. Chem. B* **2023**, *127*, 5941.
(30) Jacobson, L. D.; Herbert, J. M. Polarization-Bound Quasi-Continuum States Are Responsible for the "Blue Tail" in the Optical Absorption Spectrum of the Aqueous Electron. *J. Am. Chem. Soc.* **2010**, *132*, 10000−10002. PMID: 20608656
(31) Cavanagh, M. C.; Martini, I. B.; Schwartz, B. J. Revisiting the pump−probe polarized transient hole-burning of the hydrated electron: Is its absorption spectrum inhomogeneously broadened? *Chem. Phys. Lett.* **2004**, *396*, 359−366.
(32) Jou, F.-Y.; Freeman, G. R. Temperature and isotope effects on the shape of the optical absorption spectrum of solvated electrons in water. *J. Phys. Chem.* **1979**, *83*, 2383−2387.
(33) Gajo, C.; Jordan, C. J. C.; Oliver, T. A. A. Two-Dimensional Electronic Spectroscopy of Rhodamine 700 Using an 8 fs Ultra-broadband Laser Source and Full-Wavelength Reference Detection. *J. Phys. Chem. A* **2025**, *129*, 3537−3551.
(34) Zuehlsdorff, T. J.; Hong, H.; Shi, L.; Isborn, C. M. Nonlinear spectroscopy in the condensed phase: The role of Duschinsky rotations and third order cumulant contributions. *J. Chem. Phys.* **2020**, *153*, 044127.
(35) Zuehlsdorff, T. J.; Montoya-Castillo, A.; Napoli, J. A.; Markland, T. E.; Isborn, C. M. Optical spectra in the condensed phase: Capturing anharmonic and vibronic features using dynamic and static approaches. *J. Chem. Phys.* **2019**, *151*, 074111.
(36) Mukamel, S. Fluorescence and absorption of large anharmonic molecules - spectroscopy without eigenstates. *J. Phys. Chem.* **1985**, *89*, 1077−1087.
(37) Schwartz, B. J.; Rossky, P. J. Pump−probe spectroscopy of the hydrated electron: A quantum molecular dynamics simulation. *J. Chem. Phys.* **1994**, *101*, 6917−6926.
(38) Schwartz, B. J.; Rossky, P. J. Hydrated electrons as a probe of local anisotropy: Simulations of ultrafast polarization-dependent spectral hole burning. *Phys. Rev. Lett.* **1994**, *72*, 3282−3285.
(39) Reid, P. J.; Silva, C.; Walhout, P. K.; Barbara, P. F. Femtosecond absorption anisotropy of the aqueous solvated electron. *Chem. Phys. Lett.* **1994**, *228*, 658−664.
(40) Doan, S. C.; Schwartz, B. J. Nature of Excess Electrons in Polar Fluids: Anion-Solvated Electron Equilibrium and Polarized Hole-Burning in Liquid Acetonitrile. *J. Phys. Chem. Lett.* **2013**, *4*, 1471−1476.
(41) Baltuška, A.; Emde, M. F.; Pshenichnikov, M. S.; Wiersma, D. A. Early-Time Dynamics of the Photoexcited Hydrated Electron. *J. Phys. Chem. A* **1999**, *103*, 10065−10082.
(42) Thaller, A.; Laenen, R.; Laubereau, A. Femtosecond spectroscopy of the hydrated electron: novel features in the infrared. *Chem. Phys. Lett.* **2004**, *398*, 459−465.
(43) Tauber, M. J.; Mathies, R. A. Structure of the Aqueous Solvated Electron from Resonance Raman Spectroscopy: Lessons from Isotopic Mixtures. *J. Am. Chem. Soc.* **2003**, *125*, 1394−1402.
(44) Rosenthal, S. J.; Schwartz, B. J.; Rossky, P. J. Calculated photon echo signals for the aqueous solvated electron: The origin of ultrafast electronic dephasing. *Chem. Phys. Lett.* **1994**, *229*, 443−448.
(45) Mukamel, S. *Principles of Nonlinear Optical Spectroscopy*; Oxford University Press, 1995.


https://doi.org/10.1021/acs.jpclett.6c01291
J. Phys. Chem. Lett. 2026, 17, 6030−6038

(46) Turi, L.; Hantal, G.; Rossky, P. J.; Borgis, D. Nuclear quantum effects in electronically adiabatic quantum time correlation functions: Application to the absorption spectrum of a hydrated electron. *J. Chem. Phys.* **2009**, *131*, 024119.
(47) Wu, Y.; Tepper, H. L.; Voth, G. A. Flexible simple point-charge water model with improved liquid-state properties. *J. Chem. Phys.* **2006**, *124*, 24503.
(48) Yeh, Y.-l.; Mou, C.-Y. Orientational Relaxation Dynamics of Liquid Water Studied by Molecular Dynamics Simulation. *J. Phys. Chem. B* **1999**, *103*, 3699−3705.
(49) Hoffman, D. J.; Fayer, M. D. CLS Next Gen: Accurate Frequency−Frequency Correlation Functions from Center Line Slope Analysis of 2D Correlation Spectra Using Artificial Neural Networks. *J. Phys. Chem. A* **2020**, *124*, 5979−5992.
(50) Zuehlsdorff, T. Spectroscopy_python_code. 2019; https://github.com/tjz21/Spectroscopy_python_code.
(51) Roberts, S. T.; Loparo, J. J.; Tokmakoff, A. Characterization of spectral diffusion from two-dimensional line shapes. *J. Chem. Phys.* **2006**, *125*, 084502.



https://doi.org/10.1021/acs.jpclett.6c01291
*J. Phys. Chem. Lett.* 2026, 17, 6030−6038